

## Electronic Supplementary Information (ESI): On the energetic efficiency of producing polyoxymethylene dimethyl ethers from CO<sub>2</sub> using electrical energy

Maximilian Held<sup>a</sup>, Yannic Tönges<sup>b</sup>, Dominik Pélerin<sup>a</sup>, Martin Härtl<sup>a</sup>, Georg Wachtmeister<sup>a</sup>, and Jakob Burger<sup>\*b</sup>

<sup>a</sup> Technical University of Munich, Institute of Internal Combustion Engines, Boltzmannstrasse 15, 85748 Garching, Germany

<sup>b</sup> Technical University of Munich, Chair of Chemical Process Engineering, Campus Straubing for Biotechnologie and Sustainability, Schulgasse 16, 94315 Straubing, Germany. E-mail: burger@tum.de

### 1 Additional information on the synthesis processes

#### 1.1 Carbon Capture.<sup>1–5</sup>

In the present work, we analyzed post-combustion capture (PCC) and direct air capture (DAC) technologies. In the following, both technologies are discussed.

Most PCC technologies rely on chemical absorption. The most popular technology is the amine scrubbing via monoethanolamine (MEA) which is already available in industrial scale.<sup>6–10</sup>

DAC technologies rely on a variety of different operating principles to separate carbon emissions from air. The most important ones are physical absorbents (e. g. the commercial products Selexol, Rectisol, Sepasolv MPE), chemical absorbents (e. g. hydroxides, carbonates), adsorbents (e. g. amines on SiO<sub>2</sub> carriers, microporous materials) and cryogenic air separation. DAC systems can be installed apart from power plants. This allows for great freedom in the search for adequate operation sites.<sup>8,9,11</sup>

Both electricity and heat demand for several CC technologies are given in Table 1.

**Table 1** Energy demand for state-of-the-art CC plants

CC Type	Technology	E / MJ per kg CO <sub>2</sub>
PCC	MEA <sup>8</sup>	1.3
PCC	MEA <sup>12</sup>	3.2...4.1
PCC	MEA <sup>13</sup>	3.4
PCC	Amine <sup>9</sup>	2...3
DAC	Class-3-Amin <sup>14</sup>	6.3 (th.) + 0.9 (el.)
DAC	NaOH/ Ca(OH) <sub>2</sub> <sup>8</sup>	9.9
DAC	NaOH/ Ca(OH) <sub>2</sub> <sup>11</sup>	10...17
DAC	NaOH, KOH <sup>15</sup>	10.8...18.0
DAC	Ca(OH) <sub>2</sub> / CaCO <sub>3</sub> <sup>11</sup>	241

As PCC reference we chose the MEA process

with the lowest energy demand.<sup>8</sup> As DAC reference we chose the only commercially available technology in Europe.<sup>14</sup>

#### 1.2 FA synthesis.

In order to derive a material balance from the information in the original work, the following assumptions are used:

The product is assumed to contain 55 wt.-% FA (the original work<sup>16</sup> suggests 40-55 wt.-%). Furthermore it is stated that the yield of the process is 90 mol-%. The composition of the waste gas is given in vol-%. We assumed that:

- The liquid feed is pure methanol.
- The gaseous feed contains exactly the stoichiometric amount of oxygen.
- The waste gas contains neither MeOH nor FA.
- There are only small traces of water in the waste gas.

Since the pressures of the units were not given we assumed a pressure of 1.4 bar for reactor and column. This assumption is based on data from comparable silver processes.<sup>17</sup>

#### 1.3 TRI synthesis.

The material balance for the TRI synthesis was calculated based on graphics given by Grützner *et al.*<sup>18</sup> and the lever rule. To calculate the mass flows  $\dot{m}_i$  of all streams we used the following levers from Fig. 6 of the original work<sup>18</sup>, indexes referring to Fig. 5 of the original work<sup>18</sup>.

Column K1:

The lever rule of the leaving streams is

$$\frac{\dot{m}_5}{\dot{m}_5 + \dot{m}_4} = \frac{\overline{M,4}}{\overline{4,5}}. \quad (1)$$

Where M describes a fictitious mixing point. M has exactly the same mass and concentration as a mixture of  $\dot{m}_3$  and  $\dot{m}_{10}$  or  $\dot{m}_4$  and  $\dot{m}_5$ .

The lever rule of the entering streams is

$$\frac{\dot{m}_{10}}{\dot{m}_{10} + \dot{m}_3} = \frac{\overline{M,3}}{\overline{3,10}}. \quad (2)$$

With the correlation between the line segments containing the mixing point M

$$\overline{M,4} = \overline{M,3} + \overline{3,4} \quad (3)$$

and the material balance of the column

$$\dot{m}_{10} + \dot{m}_3 = \dot{m}_4 + \dot{m}_5 \quad (4)$$

follows

$$\dot{m}_3 = \dot{m}_5 \cdot \frac{\overline{4,5}}{\overline{3,4}} + \dot{m}_{10} \cdot \left( \frac{\overline{3,10}}{\overline{3,4}} + 1 \right). \quad (5)$$

Based on Equation (5)  $\dot{m}_3$  is known. Equation (4) is then used to calculate  $\dot{m}_4$ .  $\dot{m}_8$  follows from the lever rule of column K2

$$\dot{m}_8 = \dot{m}_5 \cdot \frac{\overline{5,7}}{\overline{8,7}}. \quad (6)$$

$\dot{m}_{10}$  follows from the lever rule of column K3

$$\dot{m}_{10} = \dot{m}_8 \cdot \frac{\overline{9,8}}{\overline{9,10}}. \quad (7)$$

Based on these equations, the mass flows of all streams are available. The concentrations of streams 4, 7, 9, and 10 were taken from the ternary diagrams. Based on mass flow and conservation of mass, all other concentrations are calculated.

#### 1.4 MeOH synthesis

Since the flowsheet of the MeOH production process in the original work<sup>19</sup> is complex and detailed, we show a simplified flowsheet to describe only the in- and outgoing streams, see Fig. 1. However, in our calculations we used the detailed

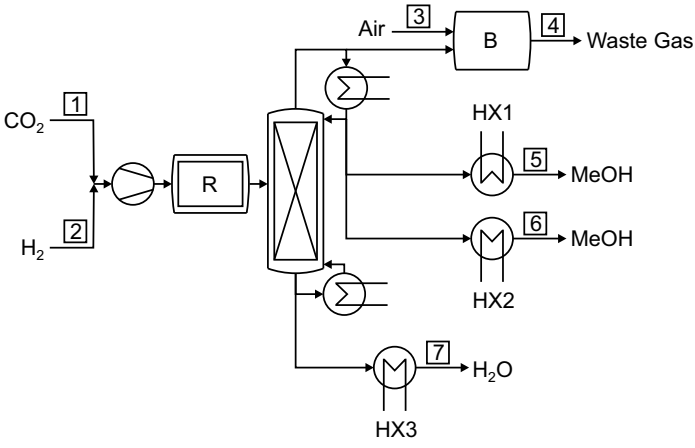


**Figure 1** Simplified flowsheet of the MeOH synthesis plant (route A and B) based on Van-Dal and Bouallou<sup>13</sup>, Pérez-Fortes *et al.*<sup>19</sup>: R = Reactor, HX = Heat exchanger, B = Burner.

data given by Pérez-Fortes *et al.*<sup>19</sup>. In the original work, pinch analysis is performed for the MeOH production as a standalone process. We also consider heat integration between the processes of

route A and B. To do so we extracted the heat duties and respective temperature levels of the process from the pinch analysis in the original work.

## 2 Overall material balance

Tables 2 to 6 show the full material balance for the complete process chain. Stream numbers refer to Fig. 1 in main manuscript. Stream 1 is always comprised of (diluted) CO<sub>2</sub>. Since three different forms of CC are considered, there are various possible compositions for stream 1. These compositions are not investigated further in the present work. All processes are scaled to the production of 1 kg OME<sub>3-5</sub> per second (equals to 3600 kg OME<sub>3-5</sub> per hour).

**Table 2** Idealized material balance for route A, stream numbers referring to Fig. 1 in main manuscript.

	1	2	3	4	5	6	7	8	9	10	11	17	18
	Mass flowrates $\dot{m}_i$ / kg per hour												
OME <sub>3-5</sub>	-	0	0	0	0	0	0	0	0	0	0	0	3600
H <sub>2</sub> O	-	7070	0	0	0	2357	0	0	1513	0	0	422	0
FA	-	0	0	0	0	0	0	0	0	0	2522	0	0
MeOH	-	0	0	0	0	0	1500	2690	0	0	0	0	0
O <sub>2</sub>	-	0	6285	0	0	0	0	0	0	1345	0	0	0
H <sub>2</sub>	-	0	0	0	786	0	0	0	0	0	0	0	0
CO <sub>2</sub>	5761	0	0	5761	0	0	0	0	0	0	0	0	0

**Table 3** Material balance for route A based on reference processes, stream numbers referring to Fig. 1 in main manuscript.

	1	2	3	4	5	6	7	8	9	10	11	17	18
	Mass flowrates $\dot{m}_i$ / kg per hour												
OME <sub>3-5</sub>	-	0	0	0	0	0	0	0	0	0	0	0	3600
H <sub>2</sub> O	-	8096	0	0	0	3000	0	0	1660	868	447	868	0
FA	-	0	0	0	0	0	0	0	0	0	2520	0	0
MeOH	-	0	0	0	0	0	1501	3005	0	0	0	0	0
O <sub>2</sub> / kg/h	-	0	7197	879	0	449	0	0	0	1251	0	0	0
H <sub>2</sub> / kg/h	-	0	0	0	900	0	0	0	70	0	0	0	0
CO <sub>2</sub>	6583	0	0	6583	0	408	0	0	411	0	0	0	0
CO	-	0	0	0	0	0	0	0	16	0	0	0	0
N <sub>2</sub>	-	0	0	2784	0	2784	0	0	4116	4116	0	0	0

**Table 4** Idealized material balance for route B, stream numbers referring to Fig. 1 in main manuscript.

	1	2	3	4	5	6	7	8	9	10	11	12	13	14	15	16	17	18
	Mass flowrates $\dot{m}_i$ / kg per hour																	
OME <sub>3-5</sub>	-	0	0	0	0	0	0	0	0	0	0	0	0	0	0	0	3600	
H <sub>2</sub> O	-	7070	0	0	0	2357	0	0	1513	0	0	422	0	0	0	0	0	
TRI	-	0	0	0	0	0	0	0	0	0	0	0	0	0	1819	0	0	
MAL	-	0	0	0	0	0	0	0	0	0	0	0	0	1781	0	0	0	
FA	-	0	0	0	0	0	0	0	0	0	703	1819	0	0	0	0	0	
MeOH	-	0	0	0	0	0	1500	2690	0	0	0	0	0	0	0	0	0	
O <sub>2</sub>	-	0	6285	0	0	0	0	0	0	0	1345	0	0	0	0	0	0	
H <sub>2</sub>	-	0	0	0	786	0	0	0	0	0	0	0	0	0	0	0	0	
CO <sub>2</sub>	5761	0	0	5761	0	0	0	0	0	0	0	0	0	0	0	0	0	
CO	-	0	0	0	0	0	0	0	0	0	0	0	0	0	0	0	0	
N <sub>2</sub>	-	0	0	0	0	0	0	0	0	0	0	0	0	0	0	0	0	

**Table 5** Material balance for route B based on reference processes, stream numbers referring to Fig. 1 in main manuscript.

	1	2	3	4	5	6	7	8	9	10	11	12	13	14	15	16	17	18
	Mass flowrates $\dot{m}_i$ / kg per hour																	
OME <sub>3-5</sub>	-	0	0	0	0	0	0	0	0	0	0	0	0	0	0	0	0	3600
H <sub>2</sub> O	-	8117	0	0	0	3008	0	0	1160	871	420	536	840	517	2	18	0	20
TRI	-	0	0	0	0	0	0	0	0	0	0	0	0	5	0	1819	0	0
MAL	-	0	0	0	0	0	0	0	0	0	0	0	0	0	1781	0	0	
FA	-	0	0	0	0	0	0	0	0	0	706	1825	3	0	0	0	0	0
MeOH	-	0	0	0	0	0	1499	3018	0	0	0	0	0	0	0	0	0	0
O <sub>2</sub>	-	0	7215	882	0	450	0	0	0	1256	0	0	0	0	0	0	0	0
H <sub>2</sub>	-	0	0	0	902	0	0	0	70	0	0	0	0	0	0	0	0	0
CO <sub>2</sub>	6600	0	0	6600	0	409	0	0	412	0	0	0	0	0	0	0	0	0
CO	-	0	0	0	0	0	0	0	16	0	0	0	0	0	0	0	0	0
N <sub>2</sub>	-	0	0	2791	0	2791	0	0	4134	4134	0	0	0	0	0	0	0	0

**Table 6** Idealized material balance for route C, stream numbers referring to Fig. 1 in main manuscript.

	1	2	3	4	5	6	7	8	9	10	11	17	18
	Mass flowrates $\dot{m}_i$ / kg per hour												
OME <sub>3-5</sub>	-	0	0	0	0	0	0	0	0	0	0	0	3600
H <sub>2</sub> O	-	7070	0	0	0	2357	0	0	0	0	0	422	0
FA	-	0	0	0	0	0	0	0	0	0	2522	0	0
MeOH	-	0	0	0	0	0	1500	2690	0	0	0	0	0
O <sub>2</sub>	-	0	6285	0	0	0	0	0	0	0	0	0	0
H <sub>2</sub>	-	0	0	0	786	0	0	0	168	0	0	0	0
CO <sub>2</sub>	5761	0	0	5761	0	0	0	0	0	0	0	0	0

### 3 Pinch analyses for route A

Pinch analysis is used to evaluate the heat integration potential of the investigated processes. Fig. 2 to 7 show the respective composite curves. A splitting of the composite curves was not considered.

#### 3.1 Scenario 1: All processes separately.

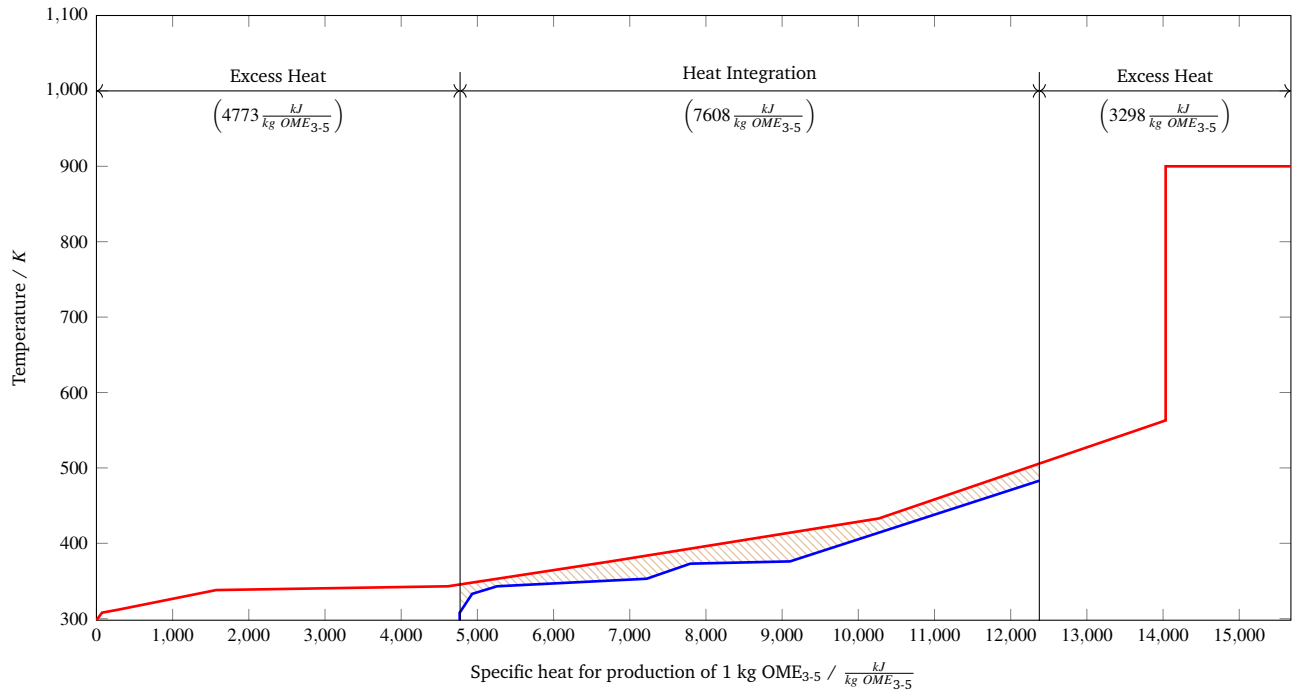


**Figure 2** Hot and cold composite curve of the MeOH synthesis plant (route A): Hot Composite Curve (red) and Cold Composite Curve (blue).

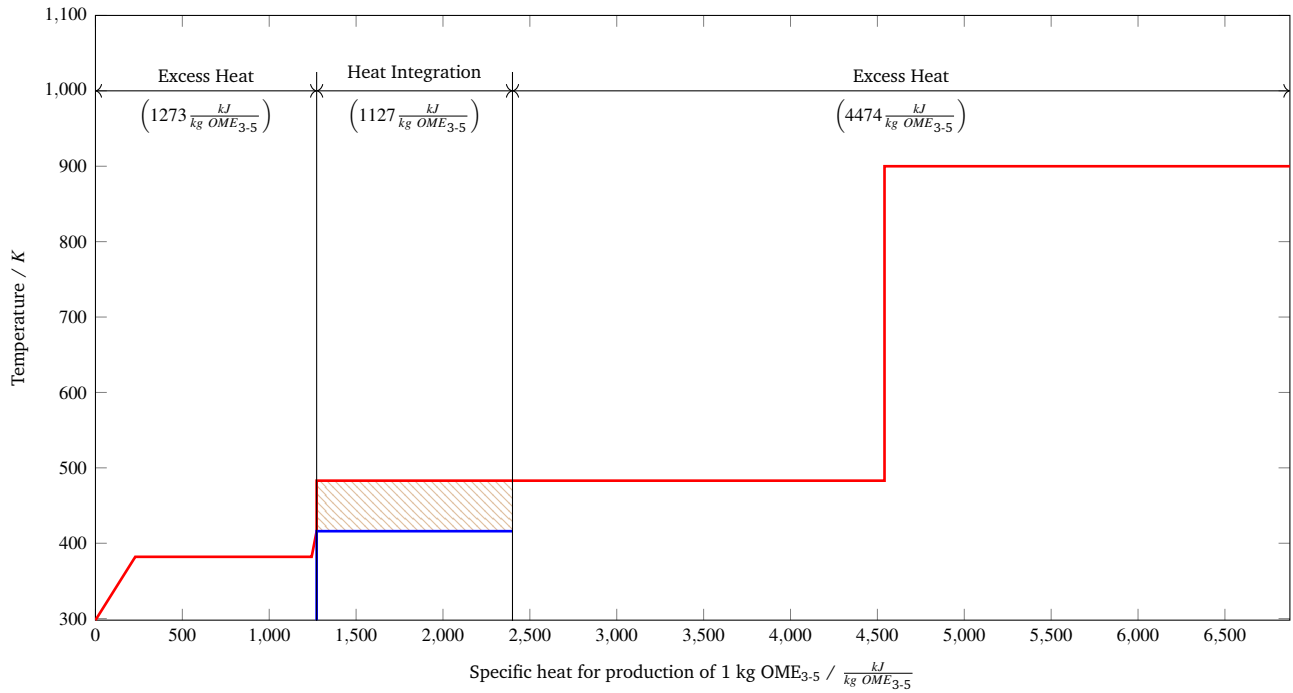


**Figure 3** Hot and cold composite curve of the FA synthesis plant (route A): Hot Composite Curve (red) and Cold Composite Curve (blue).

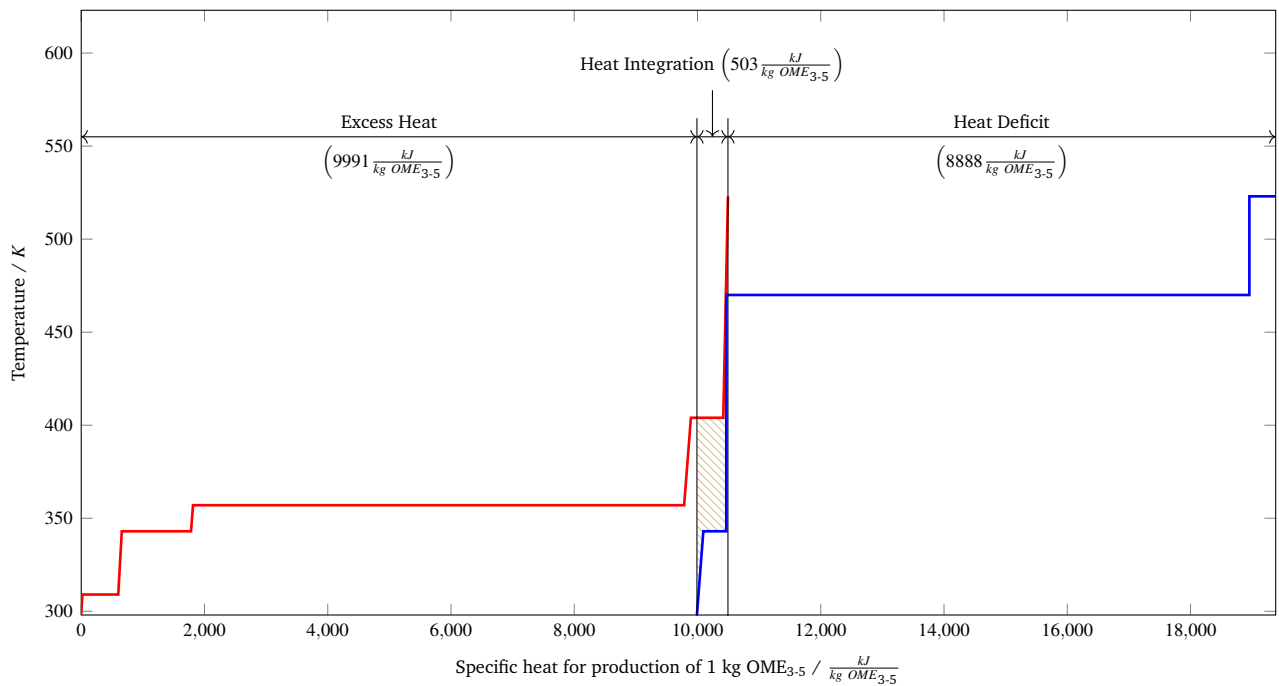
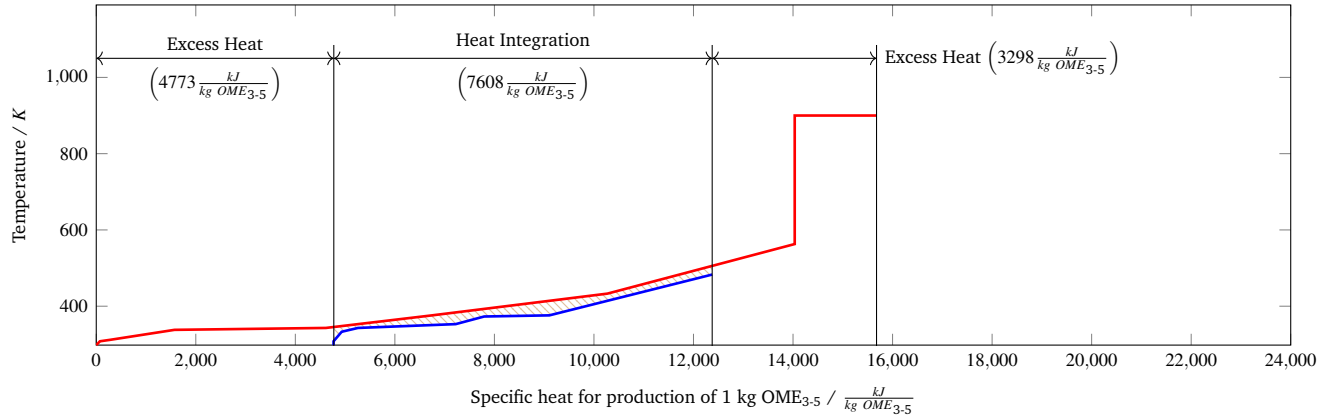


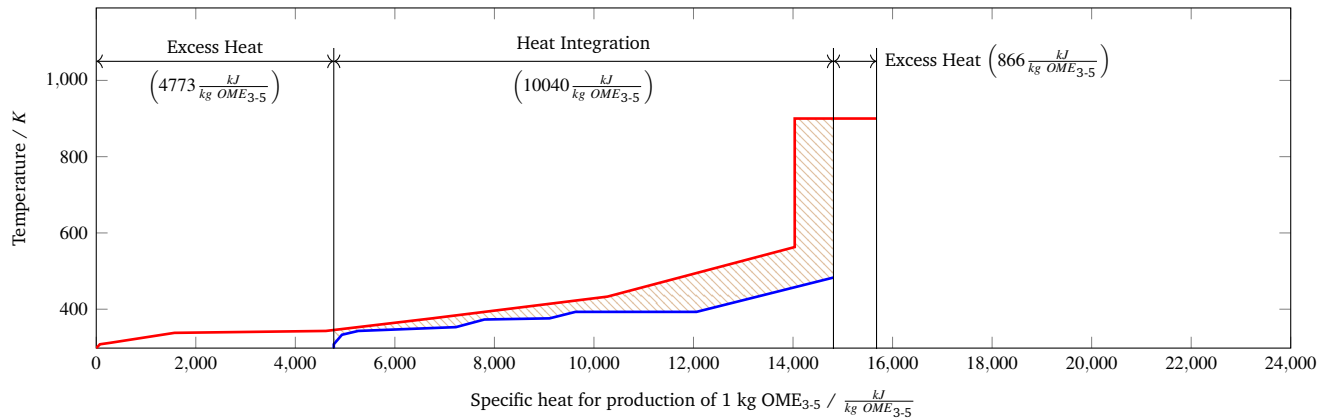
**Figure 4** Hot and cold composite curve of the OME<sub>3-5</sub> synthesis plant (route A): Hot Composite Curve (red) and Cold Composite Curve (blue).

### 3.2 Scenario 2: Two blocks.

(a) CO<sub>2</sub> supply via CPS



(b) CO<sub>2</sub> supply via PCC



(c) CO<sub>2</sub> supply via DAC

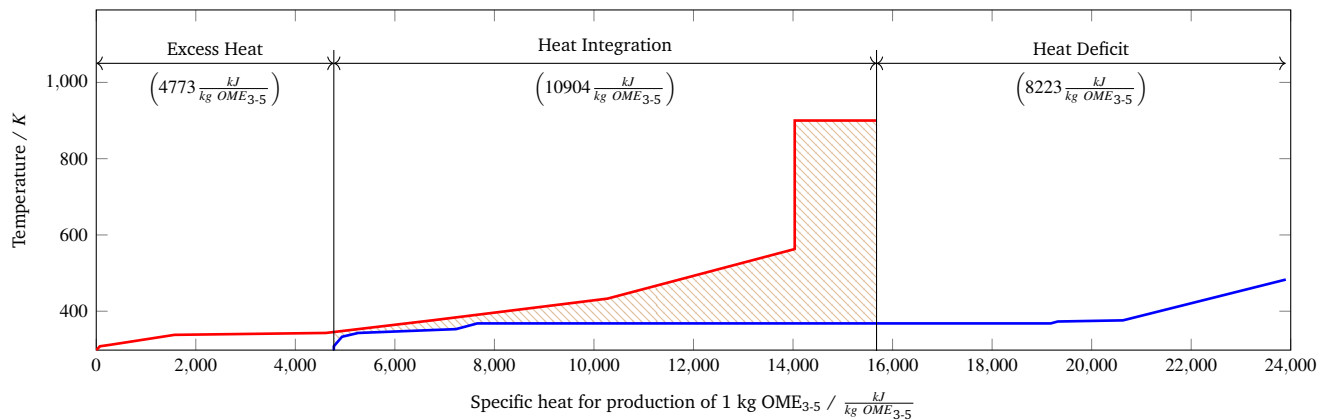


**Figure 5** Hot and cold composite curve of the first block from CC to MeOH (route A): Hot Composite Curve (red) and Cold Composite Curve (blue).

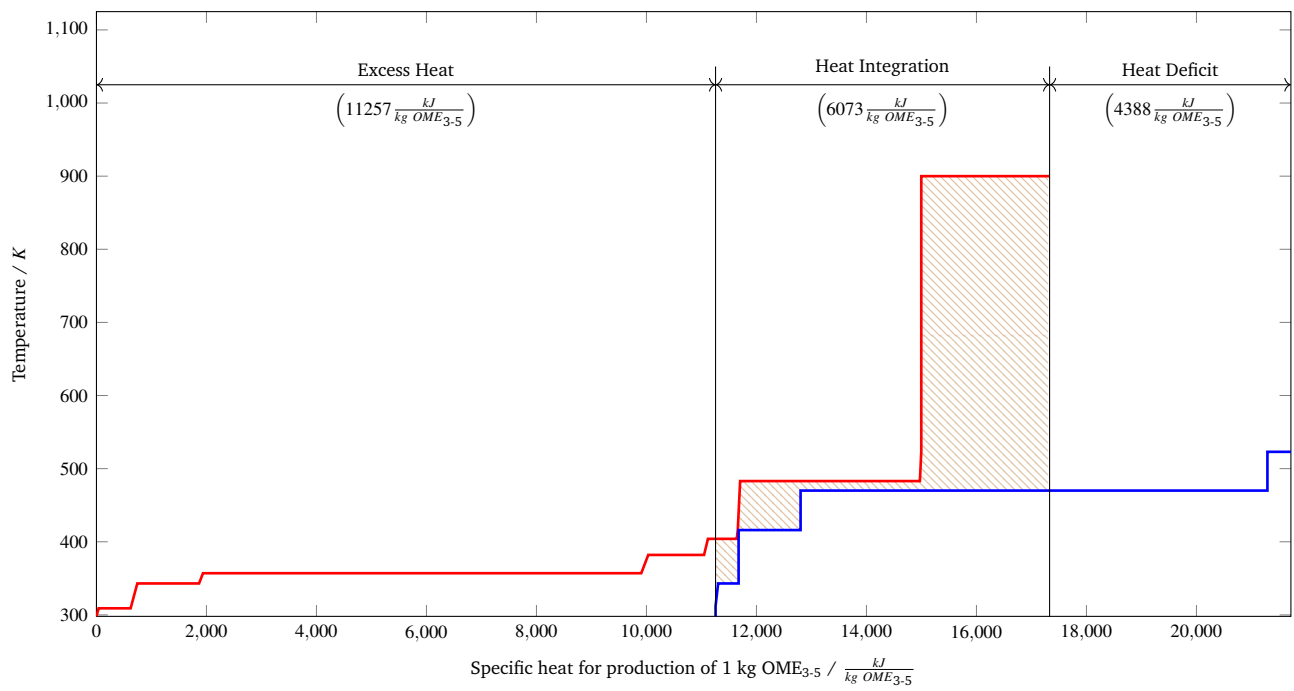
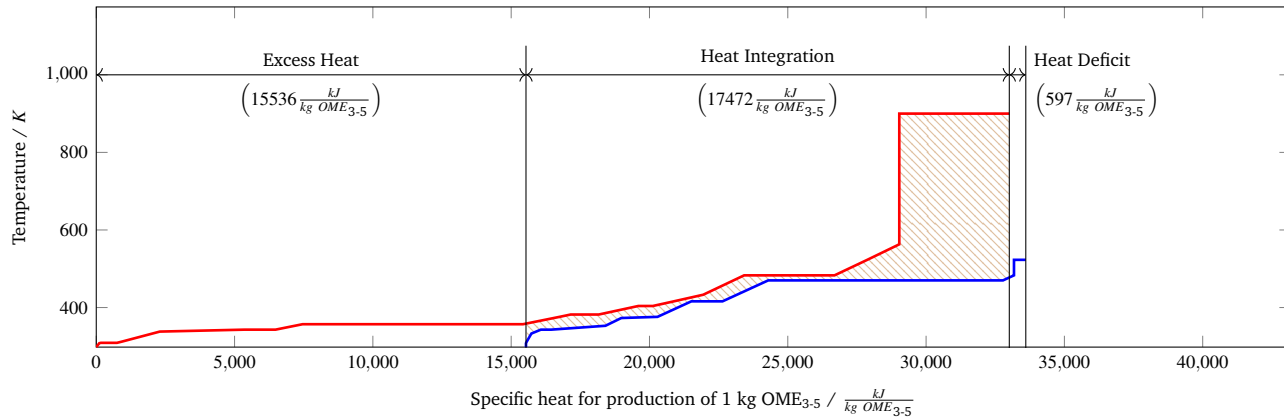


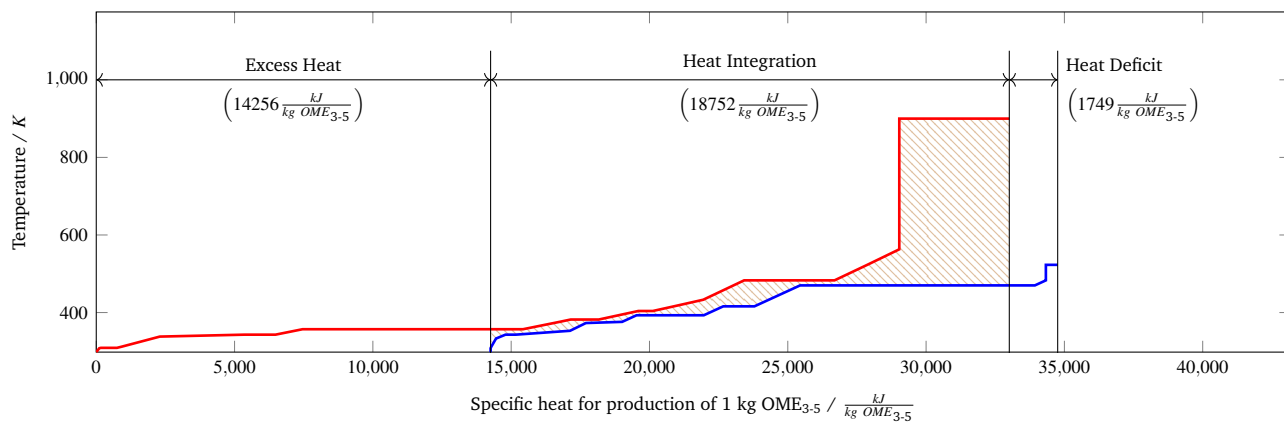
**Figure 6** Hot and cold composite curve of the second block from FA to OME<sub>3-5</sub> (route A): Hot Composite Curve (red) and Cold Composite Curve (blue).

### 3.3 Scenario 3: One block.

(a) CO<sub>2</sub> supply via CPS



(b) CO<sub>2</sub> supply via PCC



(c) CO<sub>2</sub> supply via DAC

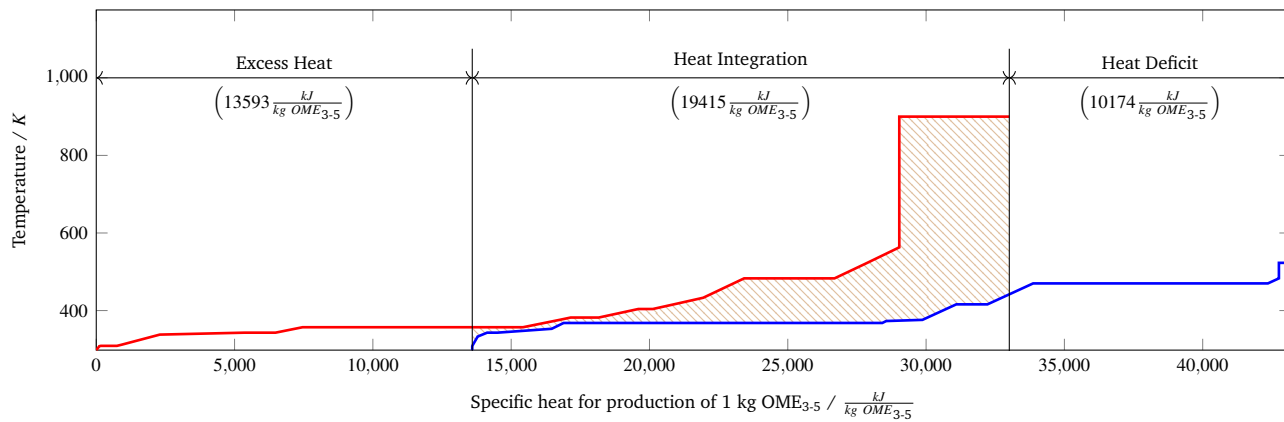


**Figure 7** Hot and cold composite curve for overall heat integration (route A): Hot Composite Curve (red) and Cold Composite Curve (blue).

## 4 Pinch analyses for route B

Pinch analysis is used to evaluate the heat integration potential of the investigated processes. Fig. 8 to 15 show the respective composite curves. A splitting of the composite curves was not considered.

### 4.1 Scenario 1: All processes separately.

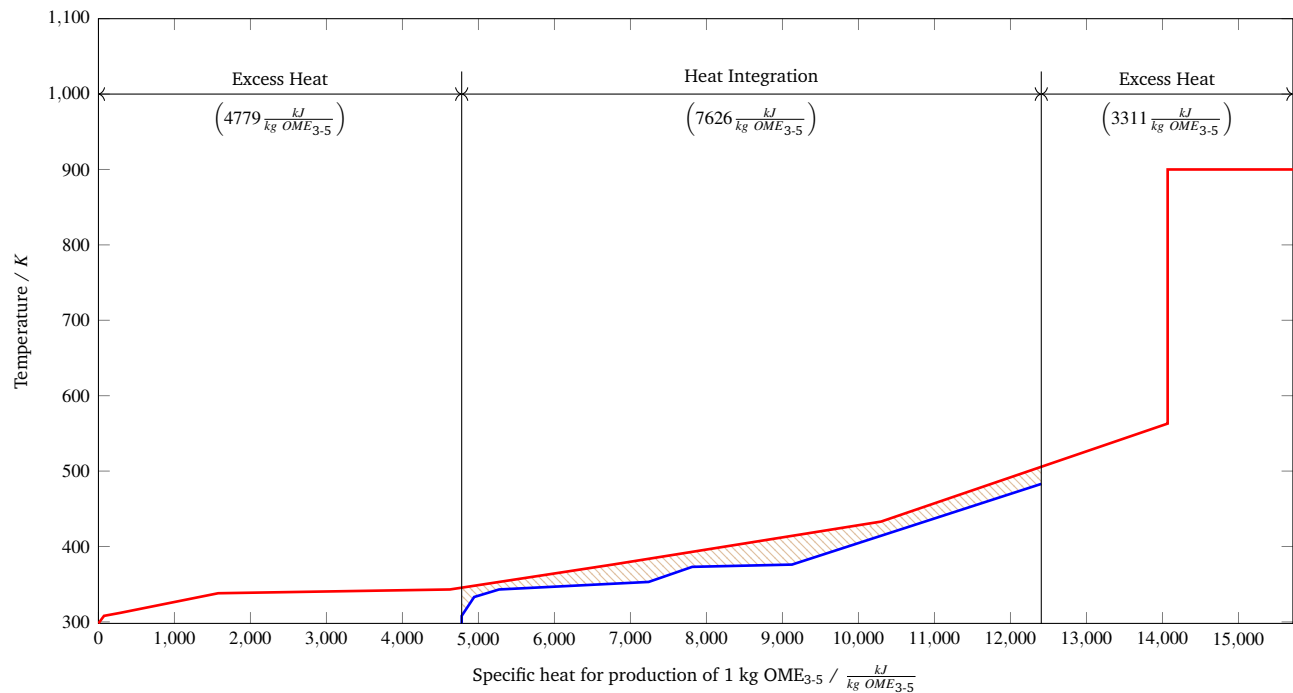


**Figure 8** Hot and cold composite curve of the MeOH synthesis plant (route B): Hot Composite Curve (red) and Cold Composite Curve (blue).

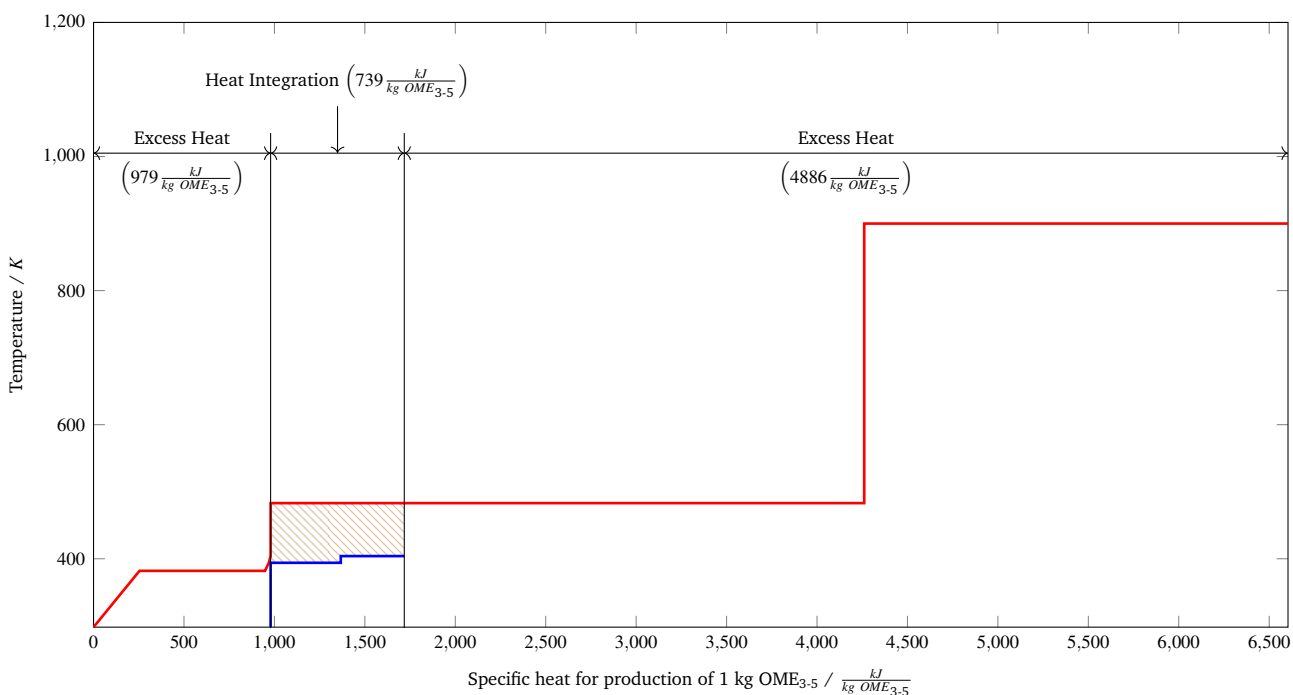


**Figure 9** Hot and cold composite curve of the FA synthesis plant (route B): Hot Composite Curve (red) and Cold Composite Curve (blue).

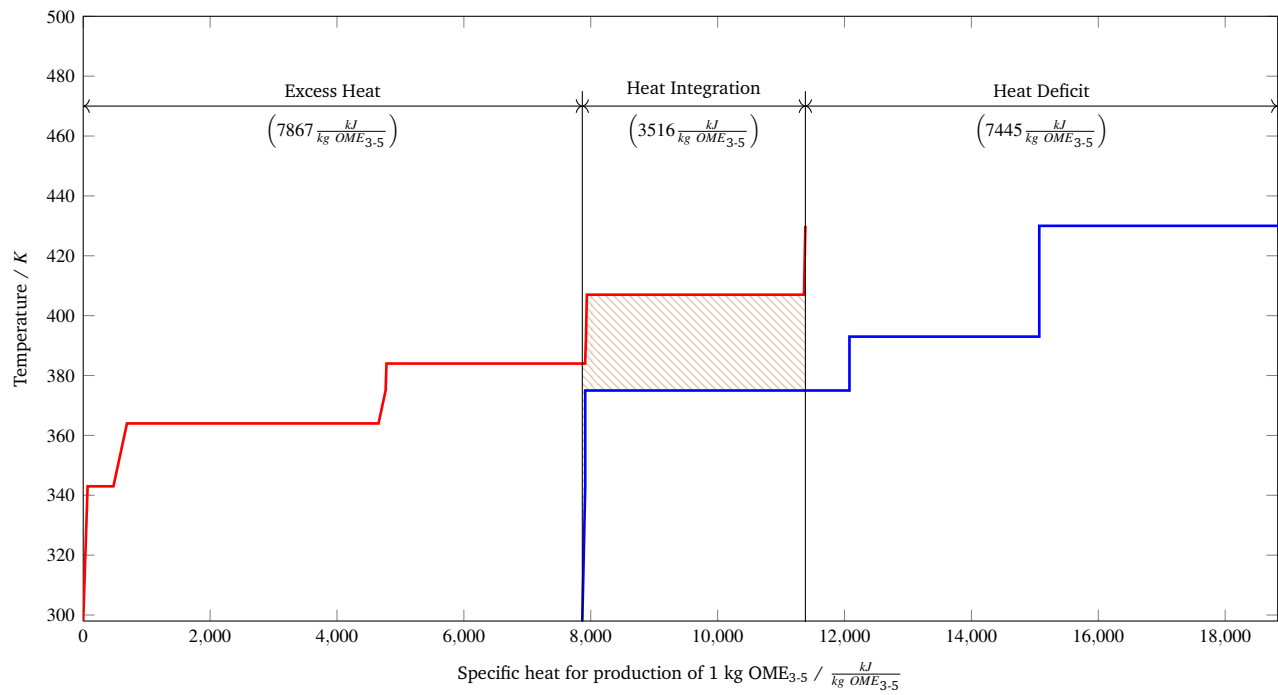


**Figure 10** Hot and cold composite curve of the TRI synthesis plant (route B): Hot Composite Curve (red) and Cold Composite Curve (blue).

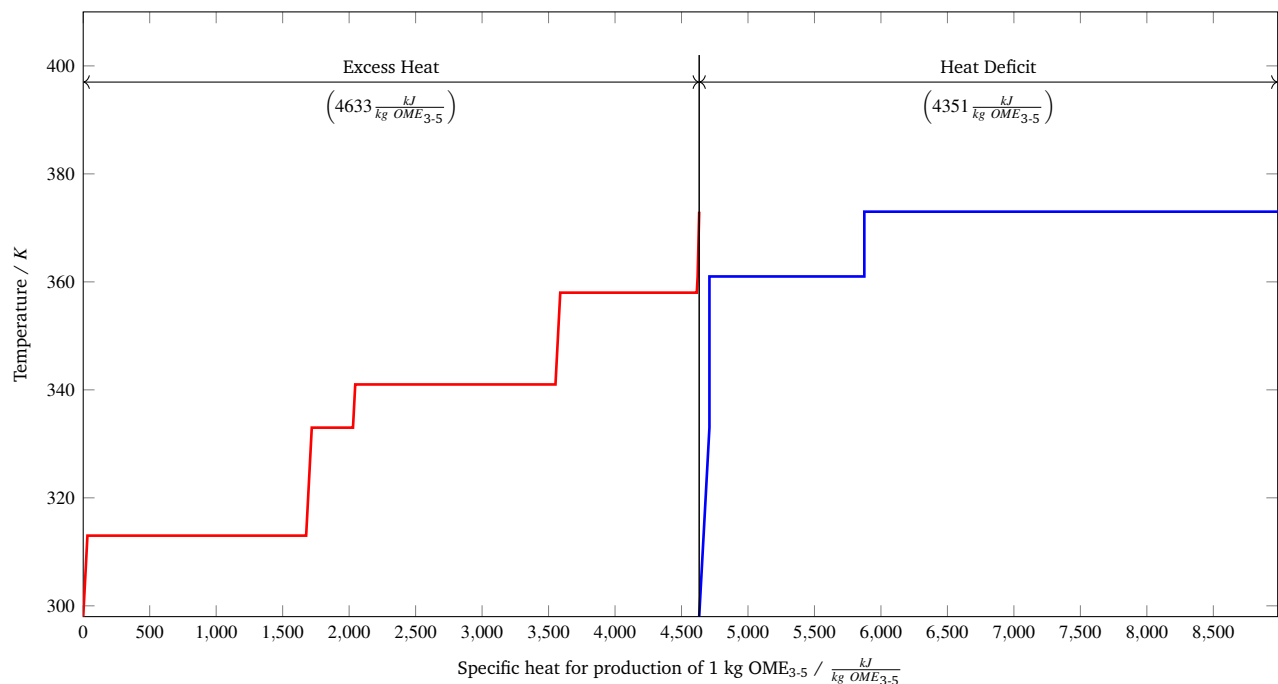


**Figure 11** Hot and cold composite curve of the MAL synthesis plant (route B): Hot Composite Curve (red) and Cold Composite Curve (blue).

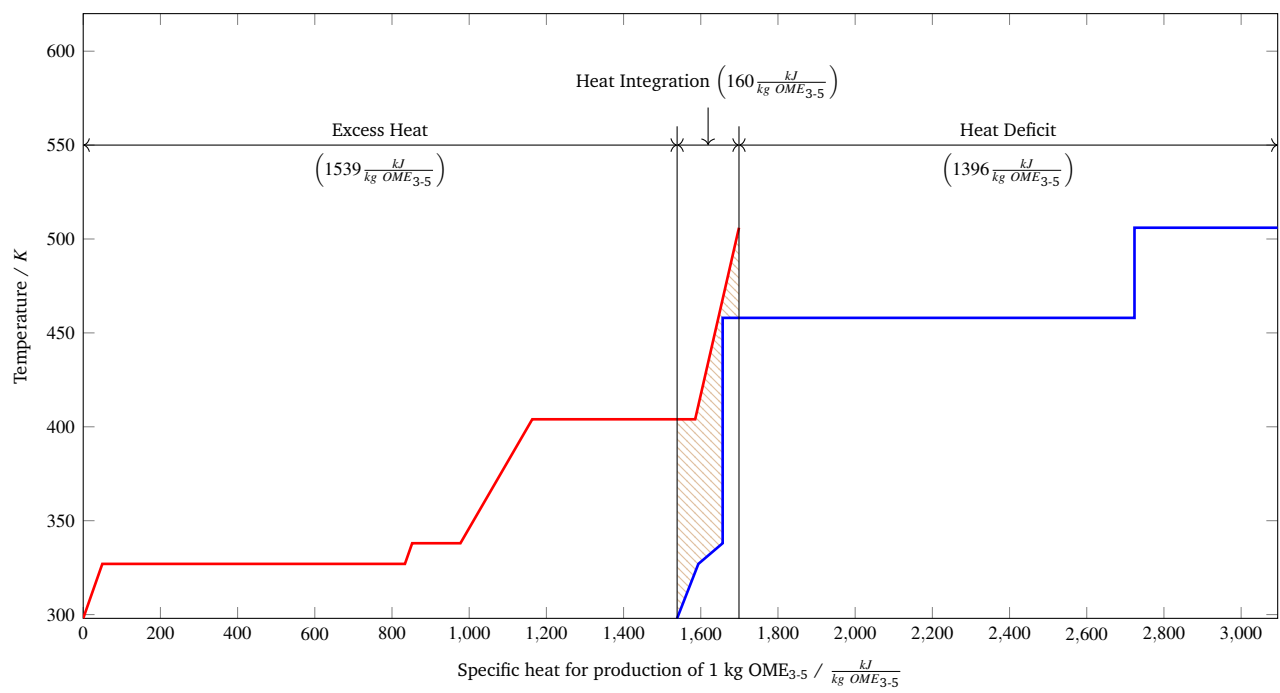
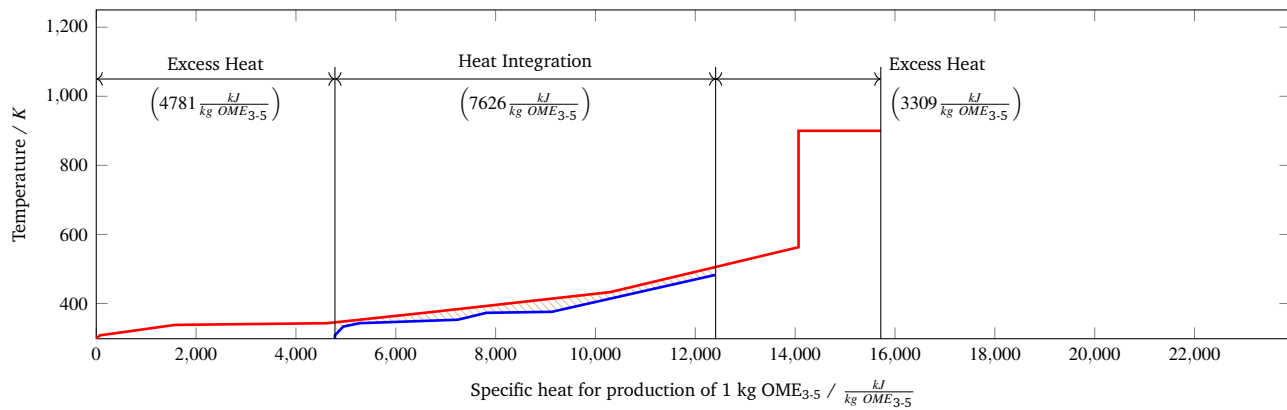


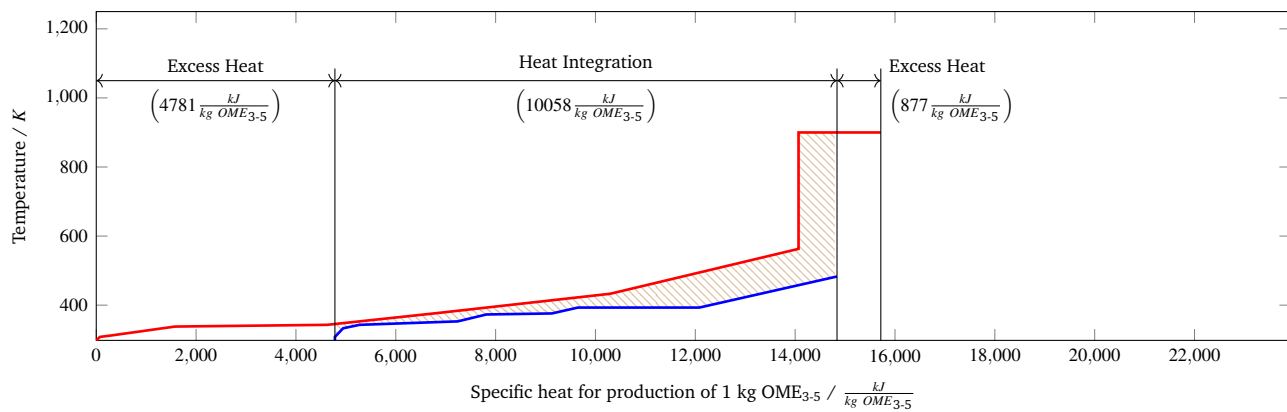
**Figure 12** Hot and cold composite curve of the OME<sub>3-5</sub> synthesis plant (route B): Hot Composite Curve (red) and Cold Composite Curve (blue).

## 4.2 Scenario 2: Two blocks.

(a) CO<sub>2</sub> supply via CPS



(b) CO<sub>2</sub> supply via PCC



(c) CO<sub>2</sub> supply via DAC

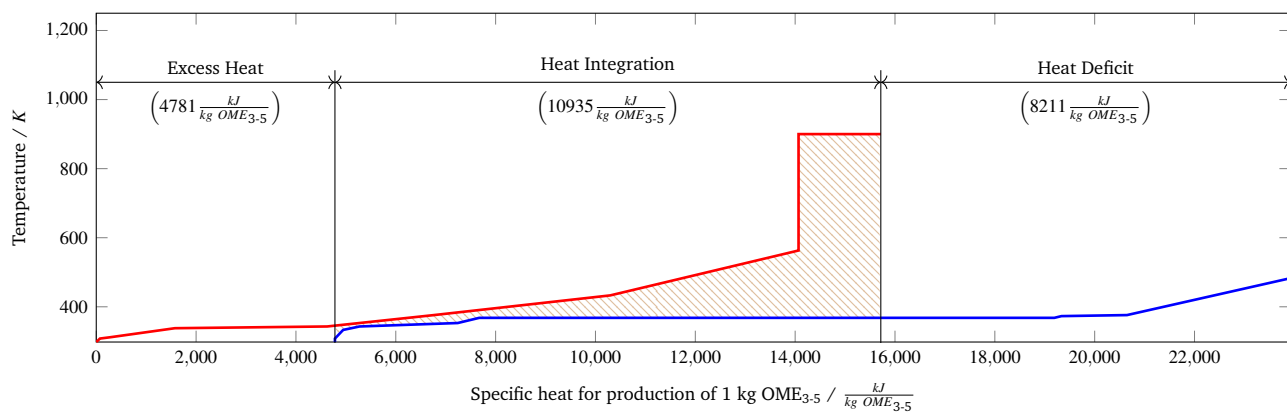


**Figure 13** Hot and cold composite curve of the first block from CC to MeOH (route B): Hot Composite Curve (red) and Cold Composite Curve (blue).

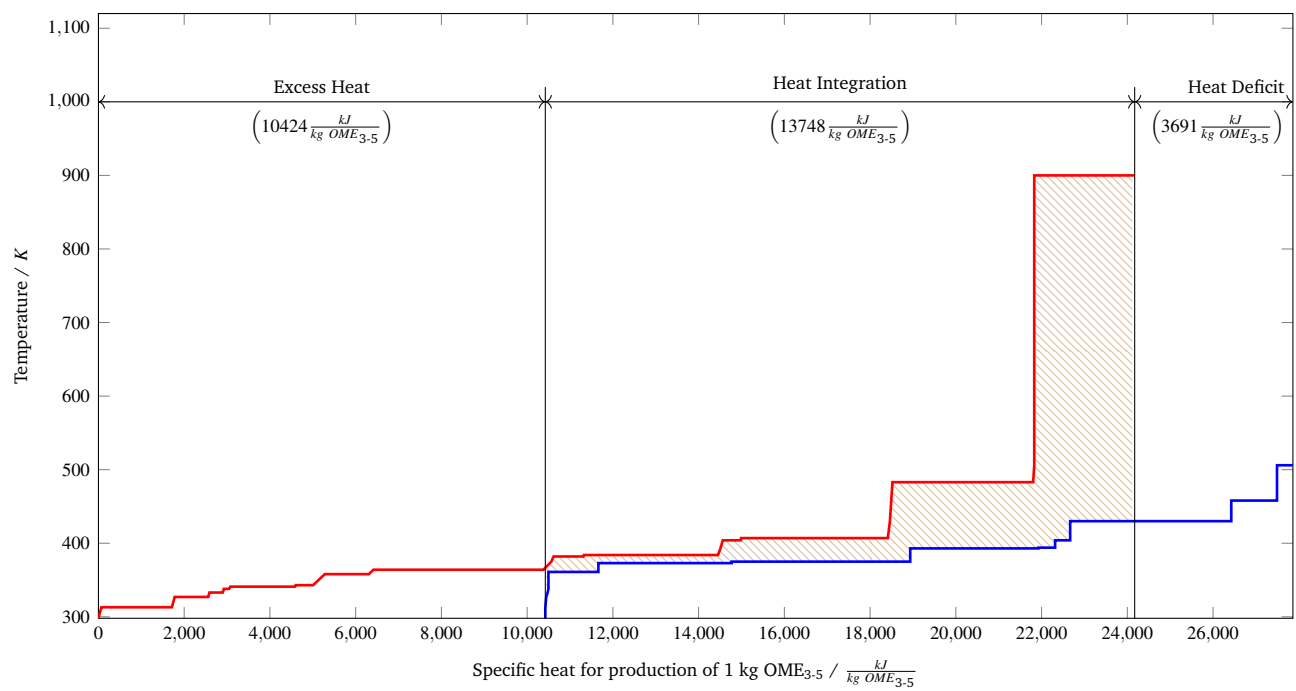
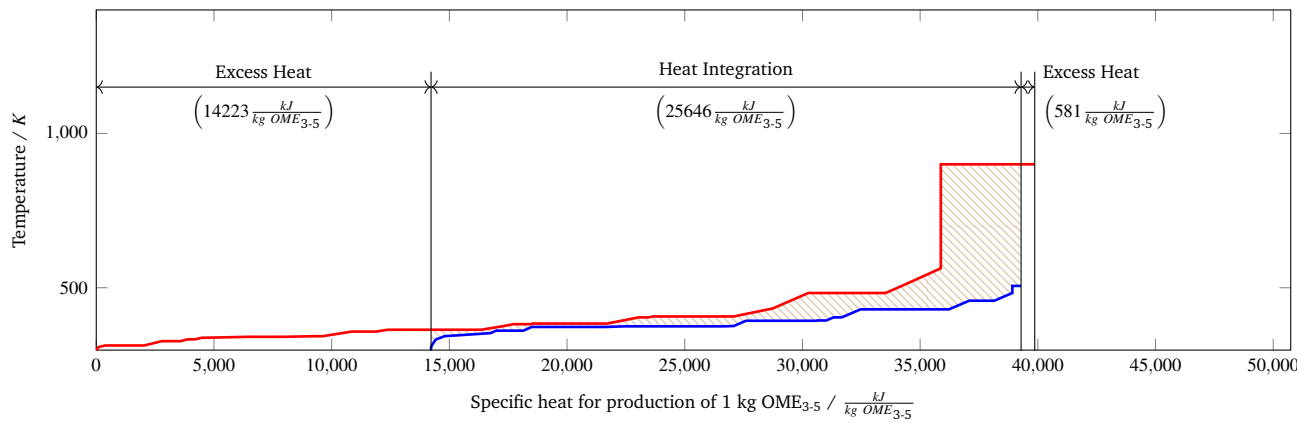


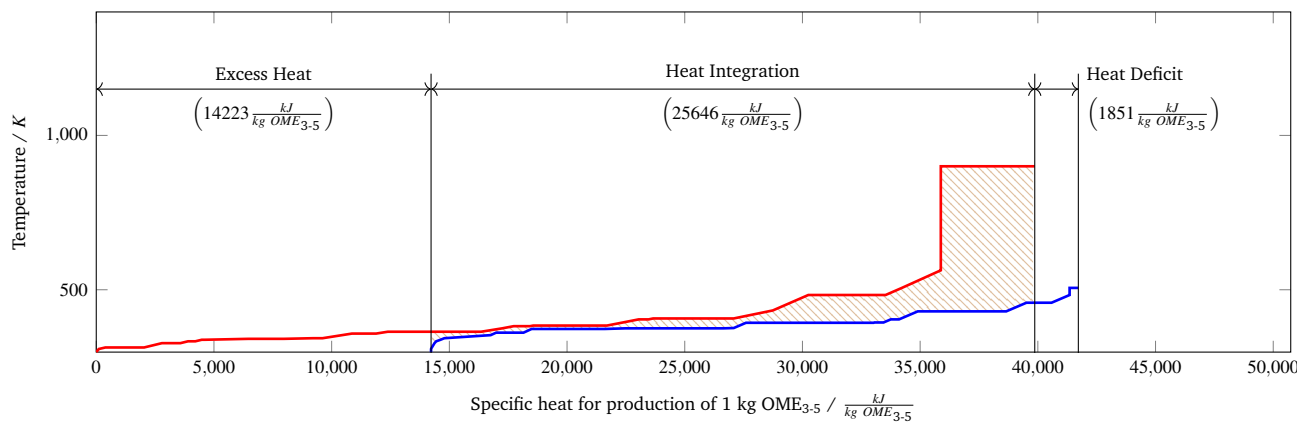
**Figure 14** Hot and cold composite curve of the second block from FA to OME<sub>3-5</sub> (route B): Hot Composite Curve (red) and Cold Composite Curve (blue).

### 4.3 Scenario 3: One block.

(a) CO<sub>2</sub> supply via CPS



(b) CO<sub>2</sub> supply via PCC



(c) CO<sub>2</sub> supply via DAC

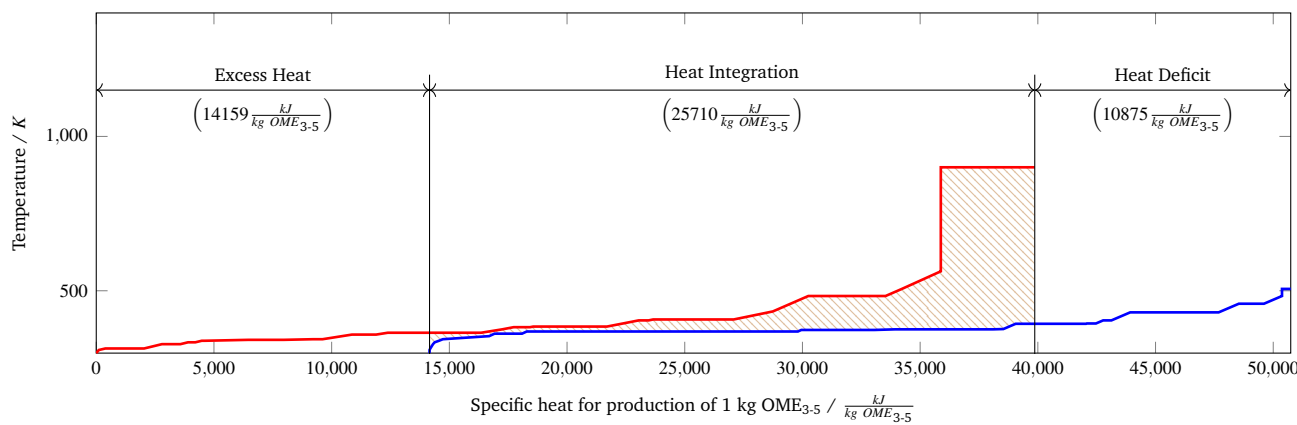


**Figure 15** Hot and cold composite curve for overall heat integration (route B): Hot Composite Curve (red) and Cold Composite Curve (blue).

## 5 Overall energy balance

Tables 7 and 8 give the overall energy balance for routes A and B for three heat integration scenarios and three CC methods.

**Table 7** Energy balance of different scenarios for route A

Scenario/ Processes	Energy / kJ per kg OME <sub>3-5</sub>		
	<i>q<sub>deficit</sub></i>	<i>q<sub>excess</sub></i>	<i>w<sub>t</sub></i>
<b>S1</b>			
EL	0	14987	50031
CC(CPS)	0	0	0
CC(PCC)	2400	0	0
CC(DAC)	11500	0	1646
MeOH	0	8071	1400
FA	0	5747	43
OME	8888	9991	0
<b>S2</b>			
EL	0	14987	50031
MeOH+CC(CPS)	0	8071	1400
MeOH+CC(PCC)	0	5639	1400
MeOH+CC(DAC)	8223	4773	3046
FA+OME	4388	11257	43
<b>S3</b>			
EL	0	14987	50031
all+CC(CPS)	597	15536	1443
all+CC(PCC)	1749	14256	1443
all+CC(DAC)	10174	13593	3089

**Table 8** Energy balance of different scenarios for route B

Scenario/ Processes	Energy / kJ per kg OME <sub>3-5</sub>		
	<i>q<sub>deficit</sub></i>	<i>q<sub>excess</sub></i>	<i>w<sub>t</sub></i>
<b>S1</b>			
EL	0	15024	50158
CC(CPS)	0	0	0
CC(PCC)	2432	0	0
CC(DAC)	11520	0	1650
MeOH	0	8090	1404
FA	0	5865	43
TRI	7445	7867	0
MAL	4351	4633	0
OME	1396	1539	0
<b>S2</b>			
EL	0	15024	50158
MeOH+CC(CPS)	0	8090	1404
MeOH+CC(PCC)	0	5658	1404
MeOH+CC(DAC)	8211	4781	3054
FA + TRI + MAL + OME <sub>3-5</sub>	3691	10424	43
<b>S3</b>			
EL	0	15024	50158
all+CC(CPS)	0	14804	1447
all+CC(PCC)	1851	14223	1447
all+CC(DAC)	10875	14159	3097

## 6 LHV efficiencies of route A and B

Tables 9 and 10 give the overall energy efficiency for all investigated cases.

**Table 9** LHV efficiency of route A for different scenarios of heat integration and different carbon sources

	<b>S1</b>	<b>S2</b>	<b>S3</b>
<b>Efficiency H<sub>2</sub>-to-OME</b>			
CPS	0.469	0.528	0.591
PCC	0.443	0.528	0.570
DAC	0.354	0.414	0.437
<b>Efficiency power-to-OME</b>			
CPS	0.313	0.339	0.363
PCC	0.301	0.339	0.355
DAC	0.257	0.288	0.299

**Table 10** LHV efficiency of route B for different scenarios of heat integration and different carbon sources

	<b>S1</b>	<b>S2</b>	<b>S3</b>
<b>Efficiency H<sub>2</sub>-to-OME</b>			
CPS	0.423	0.537	0.600
PCC	0.401	0.537	0.567
DAC	0.327	0.420	0.430
<b>Efficiency power-to-OME</b>			
CPS	0.292	0.342	0.367
PCC	0.281	0.342	0.354
DAC	0.243	0.290	0.295

## 7 Physical property data

Correlations for the vapor pressures (TRI<sup>20</sup>, MAL<sup>21</sup>, FA<sup>21</sup>, MG<sub>n</sub><sup>21</sup>, HF<sub>n</sub><sup>21</sup>, H<sub>2</sub>O<sup>21</sup>, OME<sub>2-5</sub><sup>22</sup>, OME<sub>6-10</sub><sup>23</sup>) were adopted from literature. The same holds for enthalpies of vaporization (FA<sup>24</sup>, TRI<sup>24</sup>, MAL<sup>24</sup>, OME<sub>2-10</sub><sup>23</sup>, MeOH<sup>25</sup>, H<sub>2</sub>O<sup>25</sup>, HF<sub>n</sub><sup>25</sup>, MG<sub>n</sub><sup>25</sup>, FA<sup>25</sup>) and the ideal gas heat capacities (FA<sup>24</sup>, TRI<sup>24</sup>, MAL<sup>24</sup>, OME<sub>2-10</sub><sup>23</sup>, MeOH<sup>25</sup>, H<sub>2</sub>O<sup>25</sup>, MG<sub>n</sub><sup>25</sup>, FA<sup>25</sup>, HF<sub>n</sub><sup>21</sup>).

Enthalpies of formation are adapted from the literature as well (FA<sup>24</sup>, TRI<sup>24</sup>, MAL<sup>24</sup>, OME<sub>2-10</sub><sup>23</sup>, MeOH<sup>21</sup>, H<sub>2</sub>O<sup>21</sup>, MG<sub>n</sub><sup>21</sup>, HF<sub>n</sub><sup>21</sup>).

## 8 Stream tables (MeOH to OME<sub>3-5</sub>)

### 8.1 Stream tables for single processes in route A.

Tables 11 to 13 show the stream tables of all processes in route A.

**Table 11** Stream table of the MeOH synthesis plant (route A) based on Pérez-Fortes *et al.*<sup>19</sup>, for stream numbers of Fig. 1 (asterisk indicating a different temperature in the case of heat integration of the process into preceding or subsequent process)

	1	2	3	4	5	6	7
<i>p</i> / bar	1.0	30.0	1.0	1.0	1.0	1.0	1.0
<i>T</i> / K	298	298	293	525	298	298/ 312*	298
<i>m</i> <sub>total</sub> / kg/h	6583	900	3664	4081	3005	1501	2592
Mass flowrates <i>m</i> <sub>i</sub> / kg per hour							
CO <sub>2</sub>	6583	0	0	408	0	0	0
H <sub>2</sub>	0	900	0	0	0	0	0
O <sub>2</sub>	0	0	879	449	0	0	0
N <sub>2</sub>	0	0	2784	2816	0	0	0
H <sub>2</sub> O	0	0	0	408	0	0	2592
MeOH	0	0	0	0	3005	1501	0

**Table 12** Stream table of the FA synthesis plant (route A) based on Reuss *et al.*<sup>16</sup>, stream numbers referring to Fig. 3 (a) in main manuscript (asterisk indicating a different temperature in the case of heat integration of the process into preceding or subsequent process)

	1 / 2	3	4	5	6	7	8
<i>p</i> / bar	1.0 / 1.4	1.4	1.4	1.4	1.4	1.4	1.4
<i>T</i> / K	298	298	298	298	346	483	298
<i>m</i> <sub>total</sub> / kg/h	5367	3005	3005	8372	8372	8372	868
Mass flowrates <i>m</i> <sub>i</sub> / kg per hour							
CO	0	0	0	0	0	16	0
CO <sub>2</sub>	0	0	0	0	0	411	0
O <sub>2</sub>	1251	0	0	1251	1251	0	0
N <sub>2</sub>	4116	0	0	4116	4116	4116	0
H <sub>2</sub>	0	0	0	0	0	70	0
MeOH	0	3005	3005	3005	3005	0	0
FA	0	0	0	0	0	2520	0
H <sub>2</sub> O	0	0	0	0	0	1239	868

	9	10	11	12	13	14	15
<i>p</i> / bar	1.4	1.4	1.4	1.4	1.4	1.4	1.4
<i>T</i> / K	348	381	382	382	298	416	298/ 343*
<i>m</i> <sub>total</sub> / kg/h	4658	4581	1615	1615	1615	2967	2967
Mass flowrates <i>m</i> <sub>i</sub> / kg per hour							
CO	16	0	0	0	0	0	0
CO <sub>2</sub>	411	0	0	0	0	0	0
O <sub>2</sub>	0	0	0	0	0	0	0
N <sub>2</sub>	4116	0	0	0	0	0	0
H <sub>2</sub>	70	0	0	0	0	0	0
MeOH	0	0	0	0	0	0	0
FA	0	2520	0	0	0	2520	2520
H <sub>2</sub> O	45	2062	1615	1615	1615	447	447

**Table 13** Stream table of the OME<sub>3-5</sub> synthesis plant (route A) based on Schmitz *et al.*<sup>26</sup>, stream numbers referring to Fig 3 (b) in main manuscript (asterisk indicating a different temperature in the case of heat integration of the process into preceding or subsequent process)

	1	2	3	4	5	6	7	8
<i>p</i> / bar	1.5	1.5	1.5	1.5	1.5	1.5	1.5	0.3
<i>T</i> / K	298/ 343*	343	298/ 312*	343	343	343	343	357
<i>m</i> <sub>total</sub> / kg/h	2967	2967	1501	1501	4468	23562	23562	18713
Mass flowrates <i>m</i> <sub>i</sub> / kg per hour								
FA	2520	2520	0	0	2520	10475	7957	7956
MeOH	0	0	1501	1501	1501	4661	3154	3154
H <sub>2</sub> O	447	447	0	0	447	659	1083	1083
MAL	0	0	0	0	0	3766	3766	3766
OME2	0	0	0	0	0	2754	2754	2754
OME <sub>3</sub>	0	0	0	0	0	0	1796	0
OME <sub>4</sub>	0	0	0	0	0	0	0	1105
OME <sub>5</sub>	0	0	0	0	0	0	698	0
OME <sub>6</sub>	0	0	0	0	0	471	471	0
OME <sub>7</sub>	0	0	0	0	0	330	330	0
OME <sub>8</sub>	0	0	0	0	0	212	212	0
OME <sub>9</sub>	0	0	0	0	0	141	141	0
OME <sub>n≥10</sub>	0	0	0	0	0	94	94	0
	9	10	11	12	13	14	15	16
<i>p</i> / bar	1.5	1.5	1.5	0.3	1.5	0.03	0.03	0.3
<i>T</i> / K	309	343	470	523	343	309	298	404
<i>m</i> <sub>total</sub> / kg/h	17845	17845	4847	1248	1248	868	868	3600
Mass flowrates <i>m</i> <sub>i</sub> / kg per hour								
FA	7956	7956	0	0	0	0	0	0
MeOH	3154	3154	0	0	0	0	0	0
H <sub>2</sub> O	215	215	0	0	868	868	0	0
MAL	3766	3766	0	0	0	0	0	0
OME <sub>2</sub>	2754	2754	0	0	0	0	0	0
OME <sub>3</sub>	0	0	1796	0	0	0	1796	1796
OME <sub>4</sub>	0	0	1105	0	0	0	0	1105
OME <sub>5</sub>	0	0	698	0	0	0	698	698
OME <sub>6</sub>	0	0	471	471	471	0	0	0
OME <sub>7</sub>	0	0	330	330	330	0	0	0
OME <sub>8</sub>	0	0	212	212	212	0	0	0
OME <sub>9</sub>	0	0	141	141	141	0	0	0
OME <sub>n≥10</sub>	0	0	94	94	94	0	0	0
	17							

## 9 Stream tables for single processes in route B

Tables 14 to 18 show the stream tables of all processes in route B.

**Table 14** Stream table of the MeOH synthesis plant (route B) based on Pérez-Fortes *et al.*<sup>19</sup>, for stream numbers of Fig. 1 (asterisk indicating a different temperature in the case of heat integration of the process into preceding or subsequent process)

	1	2	3	4	5	6	7
<i>p</i> / bar	1.0	30.0	1.0	1.0	1.0	1.0	1.0
<i>T</i> / K	298	298	293	525	298	298/ 312*	298
<i>m̄</i> <sub>total</sub> / kg/h	6600	902	3673	4091	3018	1499	2599
Mass flowrates <i>m̄</i> <sub>i</sub> / kg per hour							
CO <sub>2</sub>	6600	0	0	409	0	0	0
H <sub>2</sub>	0	902	0	0	0	0	0
O <sub>2</sub>	0	0	882	450	0	0	0
N <sub>2</sub>	0	0	2791	2823	0	0	0
H <sub>2</sub> O	0	0	0	409	0	0	2599
MeOH	0	0	0	0	3018	1499	0

**Table 15** Stream table of the FA synthesis plant (route B) based on Reuss *et al.*<sup>16</sup>, stream numbers referring to Fig. 3 (a) in main manuscript (asterisk indicating a different temperature in the case of heat integration of the process into preceding or subsequent process)

	1 / 2	3, 4	5	6	7	8	9
<i>p</i> / bar	1.0/ 1.4	1.4	1.4	1.4	1.4	1.4	1.4
<i>T</i> / K	298	298	298	346	483	298	348
<i>m̄</i> <sub>total</sub> / kg/h	5390	3018	8407	8407	8407	871	4678
Mass flowrates <i>m̄</i> <sub>i</sub> / kg per hour							
CO	0	0	0	0	16	0	16
CO <sub>2</sub>	0	0	0	0	412	0	412
O <sub>2</sub>	1256	0	1256	1256	0	0	0
N <sub>2</sub>	4134	0	4134	4134	4134	0	4134
H <sub>2</sub>	0	0	0	0	70	0	70
MeOH	0	3018	3018	3018	0	0	0
FA	0	0	0	0	2530	0	0
H <sub>2</sub> O	0	0	0	0	1244	871	45

	10	11,13	14	15,16	17	18,20	21,22
<i>p</i> / bar	1.4	1.4	1.4	1.4	1.4	1.4	1.4
				394/		404/	
				407/	333*	381/	343*
<i>T</i> / K	381	298	394	298*	394	298	298*
<i>m̄</i> <sub>total</sub> / kg/h	4601	567	4033	1126	2907	547	2360
Mass flowrates <i>m̄</i> <sub>i</sub> / kg per hour							
CO	0	0	0	0	0	0	0
CO <sub>2</sub>	0	0	0	0	0	0	0
O <sub>2</sub>	0	0	0	0	0	0	0
N <sub>2</sub>	0	0	0	0	0	0	0
H <sub>2</sub>	0	0	0	0	0	0	0
MeOH	0	0	0	0	0	0	0
FA	2530	0	2530	706	1824,4	0	1824,4
H <sub>2</sub> O	2070	567	1503	420	1083	547	536

**Table 16** Stream table of the TRI synthesis plant (route B) based on Grützner *et al.*<sup>18</sup>, stream numbers referring to Fig. 4 (a) in main manuscript (asterisk indicating a different temperature in the case of heat integration of the process into preceding or subsequent process)

	1	2	3	4	5	6
<i>p</i> / bar	1.0	1.0	1.0	1.0	1.0	1.0
<i>T</i> / K	298/ 343*	343	343	343	375	343
<i>m̄</i> <sub>total</sub> / kg/h	2360	2360	20842	20842	18482	18482
Mass flowrates <i>m̄</i> <sub>i</sub> / kg per hour						
TRI	0	0	0	1825	0	0
FA	1825	1825	15871	14046	14046	14046
H <sub>2</sub> O	536	536	4971	4971	4436	4436

	7	8	9	10	11	12	13
<i>p</i> / bar	1.0	4.0	4.0	4.0	2.0	2.0	2.0
<i>T</i> / K	365	430	298/ 338*	407	384	393	298
<i>m̄</i> <sub>total</sub> / kg/h	10173	1838	1838	8336	7813	522	522
Mass flowrates <i>m̄</i> <sub>i</sub> / kg per hour							
TRI	7059	1819	1819	5240	5235	5	5
FA	781	0	0	781	781	0	0
H <sub>2</sub> O	2333	18	18	2314	1797	517	517

**Table 17** Stream table of the MAL synthesis plant (route B) based on Weidert *et al.*<sup>27</sup> and<sup>28</sup>, stream numbers referring to Fig. 4 (b) in main manuscript (asterisk indicating a different temperature in the case of heat integration of the process into preceding or subsequent process)

	1	2	3	4	5	6	7
<i>p</i> / bar	2.0	2.0	2.0	2.0	2.0	2.0	2.0
	298/	298/	333*	333	333	333	333
<i>T</i> / K	333*	333	312*	333	333	333	333
<i>m̄</i> <sub>total</sub> / kg/h	1126	1126	1499	1499	2625	7282	7282
Mass flowrates <i>m̄</i> <sub>i</sub> / kg per hour							
FA	706	706	0	0	706	708	58
MeOH	0	0	1499	1499	1499	5880	4485
H <sub>2</sub> O	420	420	0	0	420	694	1085
MAL	0	0	0	0	0	0	1653

	8, 9	10	11	12	13	14	15
<i>p</i> / bar	2.0	1.0	1.0	1.0	4.0	4.0	4.0
<i>T</i> / K	341	373	298	313	358	361	298/ 338*
<i>m̄</i> <sub>total</sub> / kg/h	4657	843	843	4573	2793	1782	1782
Mass flowrates <i>m̄</i> <sub>i</sub> / kg per hour							
FA	2	3	3	0	0	0	0
MeOH	4381	0	0	310	310	0	0
H <sub>2</sub> O	274	840	840	1	0	1	1
MAL	0	0	0	4262	2482	1781	1781

**Table 18** Stream table of the OME<sub>3-5</sub> synthesis plant (route B), according to Burger *et al.*<sup>23</sup>, stream numbers referring to Fig. 3 (b) in main manuscript (asterisk indicating a different temperature in the case of heat integration of the process into preceding or subsequent process)

	1	2	3	4	5	6	7	8
<i>p</i> / bar	1.0	1.0	1.0	1.0	1.0	1.0	1.0	1.0
<i>T</i> / K	343	327	298/ 338*	338	298/ 338*	338	338	338
<i>m</i> <sub>total</sub> / kg/h	12252	6460	1781	1781	1819	1819	3600	12252
<b>Mass flowrates <i>m</i><sub>i</sub> / kg per hour</b>								
FA	32	32	0	0	0	0	0	32
TRI	491	490	0	0	1819	1819	1819	2310
MAL	3155	3155	1781	1781	0	0	1781	4936
OME <sub>2</sub>	2559	2558	0	0	0	0	0	2558
OME <sub>3</sub>	1905	209	0	0	0	0	0	209
OME <sub>4</sub>	1357	14	0	0	0	0	0	14
OME <sub>5</sub>	937	1	0	0	0	0	0	379
OME <sub>6</sub>	635	0	0	0	0	0	0	635
OME <sub>7</sub>	421	0	0	0	0	0	0	421
OME <sub>8</sub>	275	0	0	0	0	0	0	275
OME <sub>9</sub>	178	0	0	0	0	0	0	178
OME <sub>10</sub>	114	0	0	0	0	0	0	114
OME <sub>n&gt;10</sub>	192	0	0	0	0	0	0	192
	9	10	11	12	13	14	15	16
<i>p</i> / bar	-	1.0	1.0	0.3	1.0	-	-	0.3
<i>T</i> / K	-	338	458	506	338	-	-	404
<i>m</i> <sub>total</sub> / kg/h	-	6460	5792	2192	2192	-	-	3600
<b>Mass flowrates <i>m</i><sub>i</sub> / kg per hour</b>								
FA	-	32	0	0	0	-	-	0
TRI	-	490	1	0	0	-	-	1
MAL	-	3155	0	0	0	-	-	0
OME <sub>2</sub>	-	2558	1	0	0	-	-	1
OME <sub>3</sub>	-	209	1696	0	0	-	-	1696
OME <sub>4</sub>	-	14	1343	0	0	-	-	1343
OME <sub>5</sub>	-	1	937	378	378	-	-	558
OME <sub>6</sub>	-	0	635	635	635	-	-	0
OME <sub>7</sub>	-	0	421	421	421	-	-	0
OME <sub>8</sub>	-	0	275	275	275	-	-	0
OME <sub>9</sub>	-	0	178	178	178	-	-	0
OME <sub>10</sub>	-	0	114	114	114	-	-	0
OME <sub>n&gt;10</sub>	-	0	192	192	192	-	-	0

## 10 Energy demand tables (MeOH to OME<sub>3-5</sub>)

In the following subsection, the energy demands of all individual processes are given. Depending on the level of heat integration, process inputs/ outputs are either heated up/ cooled down from/ to 298 K (indicated by a) or directly integrated from/ into the preceding/ subsequent process (indicated by b). For the MeOH production, the data of the given pinch analysis in Pérez-Fortes *et al.*<sup>19</sup> is extracted graphically (Hot/ Cold Composite Curve (HCC/ CCC) sections) and augmented with additional heat sources that can be used for heat integration. The combustion temperature during burning the waste stream will exceed the normal process temperatures. Hence, the heat can be used for heat integration in any case. As the specific temperature is of no further interest, it is arbitrarily set to 900 K. The descriptions of the energy streams are referring to the units in Fig. 3 and Fig. 4 of the main manuscript.

### 10.1 Energy demand tables for single processes in route A.

**Table 19** Energy demand for the synthesis of MeOH (route A) based on Pérez-Fortes *et al.*<sup>19</sup>.  $T_{\text{in/out}}$ : inlet/ outlet temperature,  $q/w_t$ : specific heat/ electricity demand

Energy stream	$T_{\text{in}} / \text{K}$	$T_{\text{out}} / \text{K}$	$q \text{ or } w_t / \frac{\text{kJ}}{\text{kg OME}_{3-5}}$
HCC section 1	563	433	-3763
HCC section 2	433	343	-5563
HCC section 3	343	338	-3027
HCC section 4	338	308	-1391
CCC section 1	308	333	164
CCC section 2	333	343	327
CCC section 3	343	353	1963
CCC section 4	353	373	573
CCC section 5	373	376	1309
CCC section 6	376	483	3272
B (Combustion of waste product)	900	900	-1644
HX1a (MeOH as input for FA process)	312	298	-41
HX1b (MeOH as input for FA process)	312	298	-41
HX2a (MeOH as input for OME <sub>3-5</sub> process)	312	298	-19
HX2b (MeOH as input for OME <sub>3-5</sub> process)	312	312	0
HX3	374	298	-230
Compression of educts	298	298	1400

**Table 20** Energy demand for the FA synthesis plant (route A) based on Reuss *et al.*<sup>16</sup>.  $T_{\text{in/out}}$ : inlet/ outlet temperature,  $q/w_t$ : specific heat/ electricity demand

Energy stream	$T_{\text{in}} / \text{K}$	$T_{\text{out}} / \text{K}$	$q \text{ or } w_t / \frac{\text{kJ}}{\text{kg OME}_{3-5}}$
Column and evaporator HX2 fully heat-integrated	-	-	0
Reactor R	483	483	-3268
Combustion of waste product	900	900	-2333
TFE1 (thin film evaporator)	416	416	1127
CON1	382	382	-1015
HX1	298	298	0
HX3	382	298	-158
HX4a (FA input for OME <sub>3-5</sub> process)	416	298	-100
HX4b (FA input for OME <sub>3-5</sub> process)	416	343	-62
Compression of educts	298	298	43

**Table 21** Energy demand for the OME<sub>3-5</sub> synthesis plant (route A) based on Schmitz *et al.*<sup>26</sup>.  $T_{\text{in/out}}$ : inlet/ outlet temperature,  $q/w_t$ : specific heat/ electricity demand

Energy stream	$T_{\text{in}} / \text{K}$	$T_{\text{out}} / \text{K}$	$q \text{ or } w_t / \frac{\text{kJ}}{\text{kg OME}_{3-5}}$
Reactor R	343	343	-1123
Reboiler at C1	470	470	8488
Condenser at C1	357	357	-7969
Reboiler at C2	523	523	427
Condenser at C2	404	404	-525
CON1	298	298	-587
HX1a	298	343	38
HX1b	343	343	0
HX2a	298	343	66
HX2b	312	343	47
HX3	343	343	372
HX4	523	343	-115
HX5	404	298	-180

## 10.2 Energy demand tables for single processes in route B.

**Table 22** Energy demand for the synthesis of MeOH (route B) based on Pérez-Fortes *et al.*<sup>19</sup>.  $T_{\text{in/out}}$ : inlet/ outlet temperature,  $q/w_t$ : specific heat/ electricity demand

Energy stream	$T_{\text{in}} / \text{K}$	$T_{\text{out}} / \text{K}$	$q \text{ or } w_t / \frac{\text{kJ}}{\text{kg OME}_{3.5}}$
HCC section 1	563	433	-3772
HCC section 2	433	343	-5577
HCC section 3	343	338	-3034
HCC section 4	338	308	-1394
CCC section 1	308	333	164
CCC section 2	333	343	328
CCC section 3	343	353	1968
CCC section 4	353	373	574
CCC section 5	373	376	1312
CCC section 6	376	483	3280
B (Combustion of waste product)	900	900	-1648
HX1a (MeOH as input for FA process)	312	298	-41
HX1b (MeOH as input for FA process)	312	298	-41
HX2a (MeOH as input for MAL process)	312	298	-19
HX2b (MeOH as input for MAL process)	312	312	0
HX3	374	298	-231
Compression of educts	298	298	1404

**Table 23** Energy demand for the FA synthesis plant (route B) based on Reuss *et al.*<sup>16</sup>.  $T_{\text{in/out}}$ : inlet/ outlet temperature,  $q/w_t$ : specific heat/ electricity demand

Energy stream	$T_{\text{in}} / \text{K}$	$T_{\text{out}} / \text{K}$	$q \text{ or } w_t / \frac{\text{kJ}}{\text{kg OME}_{3.5}}$
Column and evaporator HX2 fully heat-integrated	-	-	0
Reactor R	483	483	-3282
Combustion of waste product	900	900	-2343
TFE (thin film evaporator)	393	393	702
CON1	373	373	-702
HX1	298	298	0
HX3	381	298	-55
HX4	381	298	-54
HX5a (FA input for MAL process)	394	298	-70
HX5b (FA input for MAL process)	394	333	-45
HX6a (FA input for TRI process)	404	298	-106
HX6b (FA input for TRI process)	404	343	-61
Compression of educts	298	298	43

**Table 24** Energy demand for the TRI synthesis plant (route B) based on Grützner *et al.*<sup>18</sup>.  $T_{\text{in/out}}$ : inlet/ outlet temperature,  $q/w_t$ : specific heat/ electricity demand

Energy stream	$T_{\text{in}} / \text{K}$	$T_{\text{out}} / \text{K}$	$q \text{ or } w_t / \frac{\text{kJ}}{\text{kg OME}_{3.5}}$
Reactor R	343	343	-407
Reboiler at C1	375	375	4165
Condenser at C1	364	364	-3965
Reboiler at C2	430	430	3758
Condenser at C2	407	407	-3423
Reboiler at C3	393	393	2992
Condenser at C3	384	384	-3131
HX1a	298	343	46
HX1b	343	343	0
HX2	375	343	-276
HX3a	430	298	-124
HX3b	430	338	-91
HX4	393	298	-57

**Table 25** Energy demand for the MAL synthesis plant (route B) based on Weidert *et al.*<sup>27</sup> and Drunsel *et al.*<sup>28</sup>.  $T_{\text{in/out}}$ : inlet/ outlet temperature,  $q/w_t$ : specific heat/ electricity demand

Energy stream	$T_{\text{in}} / \text{K}$	$T_{\text{out}} / \text{K}$	$q \text{ or } w_t / \frac{\text{kJ}}{\text{kg OME}_{3.5}}$
Reactor R	333	333	-310
Reboiler at C1	373	373	3109
Condenser at C1	313	313	-1645
Reboiler at C2	361	361	1165
Condenser at C2	358	358	-1027
CON1	341	341	-1506
HX1a	298	333	26
HX1b	333	333	0
HX2a	298	333	51
HX2b	312	333	31
HX3	373	298	-73
HX4a	361	298	-72
HX4b	361	338	-28

**Table 26** Energy demand for the OME<sub>3.5</sub> synthesis plant (route B), according to Burger *et al.*<sup>23</sup>.  $T_{\text{in/out}}$ : inlet/ outlet temperature,  $q/w_t$ : specific heat/ electricity demand

Energy stream	$T_{\text{in}} / \text{K}$	$T_{\text{out}} / \text{K}$	$q \text{ or } w_t / \frac{\text{kJ}}{\text{kg OME}_{3.5}}$
Reactor R	338	338	-125
Reboiler at C1	458	458	1067
Condenser at C1	327	327	-784
Reboiler at C2	506	506	371
Condenser at C2	404	404	-422
HX1a	298	338	44
HX1b	338	338	0
HX2a	298	338	32
HX2b	338	338	0
HX3	327	338	42
HX4	506	338	-187
HX5	404	298	-181

## 11 Abbreviations

B	Burner (in Flowsheets)
C	Rectification Column (in Flowsheets)
CC	Carbon Capture
CCC	Cold Composite Curve (in Pinch Analyses)
CCU	Carbon Capture and Utilization
CPS	CO <sub>2</sub> from Point Sources
DAC	Direct Air Capture
DME	Dimethyl Ether
FA	Formaldehyde
FCV	Fuel Cell Vehicle
HCC	Hot Composite Curve (in Pinch Analyses)
HF	Hemiformal
HF <sub>n</sub>	Polyoxymethylene hemiformal
MEA	Monoethanol amine
MeOH	Methanol
MG	Methylene glycole
MG <sub>n</sub>	Polyoxymethylene glycole
MAL	Polyoxymethylene ether
OME <sub>n</sub>	Polyoxymethylene dimethyl ether
PCC	Post-Combustion Capture
R	Reactor (in Flowsheets)
TFE	Thin Film Evaporator (in Flowsheets)
TRI	Trioxane

## References

- [1] M. E. Boot-Handford, J. C. Abanades, E. J. Anthony, M. J. Blunt, S. Brandani, N. Mac Dowell, J. R. Fernández, M.-C. Ferrari, R. Gross, J. P. Hallett, R. S. Haszeldine, P. Heptonstall, A. Lyngfelt, Z. Makuch, E. Mangano, R. T. J. Porter, M. Pourkashanian, G. T. Rochelle, N. Shah, J. G. Yao and P. S. Fennell, *Energy & Environmental Science*, 2014, **7**, 130–189.
- [2] M. Bui, C. S. Adjiman, A. Bardow, E. J. Anthony, A. Boston, S. Brown, P. S. Fennell, S. Fuss, A. Galindo, L. A. Hackett, J. P. Hallett, H. J. Herzog, G. Jackson, J. Kemper, S. Krevor, G. C. Maitland, M. Matuszewski, I. S. Metcalfe, C. Petit, G. Puxty, J. Reimer, D. M. Reiner, E. S. Rubin, S. A. Scott, N. Shah, B. Smit, J. P. M. Trusler, P. Webley, J. Wilcox and N. Mac Dowell, *Energy & Environmental Science*, 2018, **11**, 1062–1176.
- [3] A. Goeppert, M. Czaun, G. K. Surya Prakash and G. A. Olah, *Energy & Environmental Science*, 2012, **5**, 7833.
- [4] P. Markewitz, W. Kuckshinrichs, W. Leitner, J. Linssen, P. Zapp, R. Bongartz, A. Schreiber and T. E. Müller, *Energy & Environmental Science*, 2012, **5**, 7281.
- [5] X. Zhang, X. Zhang, H. Dong, Z. Zhao, S. Zhang and Y. Huang, *Energy & Environmental Science*, 2012, **5**, 6668.
- [6] P. Markewitz, W. Kuckshinrichs, W. Leitner, J. Linssen, P. Zapp, R. Bongartz, A. Schreiber and T. E. Müller, *Energy & Environmental Science*, 2012, **5**, 7281.
- [7] E. J. Novek, E. Shaulsky, Z. S. Fishman, L. D. Pfefferle and M. Elimelech, *Environmental Science & Technology Letters*, 2016, **3**, 291–296.
- [8] R. Socolow, M. Desmond, R. Aines, J. Blackstock, O. Bolland, T. Kaarsberg, L. Nathan, M. Mazzotti, A. Pfeffer, K. Sawyer, J. Siirola, B. Smit and J. Wilcox, *American Physical Society*, 2011.
- [9] B. E. Launder and J. M. T. Thompson, *Capturing CO<sub>2</sub> from the atmosphere: rationale and process design considerations*, Cambridge Univ. Press, 2010.
- [10] T. Kuramochi, A. Ramírez, W. Turkenburg and A. Faaij, *Progress in Energy and Combustion Science*, 2012, **38**, 87–112.
- [11] A. Goeppert, M. Czaun, G. K. Surya Prakash and G. A. Olah, *Energy & Environmental Science*, 2012, **5**, 7833.
- [12] R. J. Pearson, M. D. Eisaman, J. W. G. Turner, P. P. Edwards, Z. Jiang, V. L. Kuznetsov, K. A. Littau, L. di Marco and S. R. G. Taylor, *Proceedings of the IEEE*, 2012, **100**, 440–460.
- [13] É. S. Van-Dal and C. Bouallou, *Journal of Cleaner Production*, 2013, **57**, 38–45.
- [14] Climeworks AG, *Website of Climeworks AG*, 2017, <http://www.climeworks.com/>.
- [15] S. Schiebahn, T. Grube, M. Robinius, V. Tietsche, B. Kumar and D. Stolten, *International Journal of Hydrogen Energy*, 2015, **40**, 4285–4294.
- [16] G. Reuss, W. Disteldorf, A. O. Gamer and A. Hilt, *Ullmann's Encyclopedia of Industrial Chemistry*, 2000.
- [17] A. K. Kralj, *Energy*, 2010, **35**, 2528–2534.
- [18] T. Grützner, H. Hasse, N. Lang, M. Siegert and E. Ströfer, *Chemical Engineering Science*, 2007, **62**, 5613–5620.
- [19] M. Pérez-Fortes, J. C. Schöneberger, A. Boulamanti and E. Tzimas, *Applied Energy*, 2016, **161**, 718–732.
- [20] M. Albert, H. Hasse, C. Kuhnert and G. Maurer, *Journal of Chemical & Engineering Data*, 2005, **50**, 1218–1223.
- [21] C. Kuhnert, M. Albert, S. Breyer, I. Hahnenstein, H. Hasse and G. Maurer, *Industrial & Engineering Chemistry Research*, 2006, **45**, 5155–5164.
- [22] R. H. Boyd, *Journal of Polymer Science*, 1961, **50**, 133–141.
- [23] J. Burger, E. Ströfer and H. Hasse, *Chemical Engineering Research and Design*, 2013, **91**, 2648–2662.

- [24] Department of Chemical Engineering, Brigham University, Provo, Utah, *Thermophysical Properties Laboratory Project 801*, 2009.
- [25] M. Albert, *PhD Thesis: Thermodynamische Eigenschaften formaldehydhaltiger Mischungen*, University Kaiserslautern, 1999.
- [26] N. Schmitz, E. Ströfer, J. Burger and H. Hasse, *Industrial and Engineering Chemistry Research*, 2017, **56**, 11519–11530.
- [27] J.-O. Weidert, J. Burger, M. Renner, S. Blagov and H. Hasse, *Industrial and Engineering Chemistry Research*, 2017, **56**, 575–582.
- [28] J.-O. Drunsel, M. Renner and H. Hasse, *Chemical Engineering Research and Design*, 2012, **90**, 696–703.